Lagrangian chaos and correlated Lévy flights in a three-dimensional, time-independent flow

M.A. Fogleman†, M.J. Fawcett, and T. H. Solomon*
Department of Physics, Bucknell University, Lewisburg, PA 17837
(June 22, 2000)

A novel, three-dimensional, time-independent fluid flow is presented in which passive tracers follow chaotic trajectories composed of correlated Lévy flights with varying velocities. The flow is the superposition of two chains of alternating vortices, one horizontal and the other vertical. Long-range transport is superdiffusive with a growth exponent that – for long times – can be related to flight length statistics. An intermediate scaling regime is also found with a different exponent, which can be explained by considering correlations between the flights.

05.40.Fb, 47.52.+j, 94.10.Lf, 05.45.Pq

It is well known that a simple, ordered fluid flow can have particle trajectories that are *chaotic* in the sense that nearby trajectories separate exponentially in time. [1] There have been several studies of this phenomena – referred to as *Lagrangian chaos* – in two-dimensional (2D) time-periodic flows. [2,3] If the flow is three-dimensional (3D), chaotic trajectories are possible even if the flow is *time independent*, as was first explained by Arnol'd in 1965. [4] Arnol'd's theory, however applies only to inviscid flows that satisfy the Beltrami condition $\vec{\nabla} \times \vec{u} = \lambda \vec{u}$, where $\vec{u}$ is the velocity field and λ is a constant. These conditions are very difficult to achieve in a real fluid flow; consequently, there has been limited interest in Lagrangian chaos in 3D, time-independent flows. Recently, however, Yannacopoulos et al. [5] proposed that Lagrangian chaos is possible in a much wider variety of 3D, time-independent flows; most significantly, the flow need not be invisicid, and the requirement that the flow satisfy the Beltrami condition is eliminated. This theory further proposes that chaos will be most commonly observed in regions where the diagnostic $|\vec{\nabla} \times \vec{\omega}|^2$ is largest.

Lagrangian chaos leads to significant enhancements in long-range transport. The variance of a distribution of tracers typically grows as a power law: $< r^2 > \sim t^\gamma$. According to the Central Limit Theorem, the transport will be normally diffusive ($\gamma = 1$) if there are finite length and time scales to the motions of the tracers. On the other hand, superdiffusive ($\gamma > 1$) transport is possible if the trajectories are characterized by *Lévy flights* – long distance "jumps " (between regions with relatively little motion) with a wide range of lengths and durations and no finite scale. [6] Lévy flights due to Lagrangian chaos have been found experimentally [7] in a 2D flow with well-defined jet regions (regions with open flow) that carry tracers long distances before they stick to vortex islands.

In this letter, we present a novel model of an experimentally-realizeable flow that illustrates Lagrangian chaos in a 3D, time-independent flow that does not satisfy the Beltrami condition. We consider this model flow to be ideal for this type of study due both to its simplicity and to its rich transport properties, which will be illustrated in this letter. Numerical simulations of motion in this model reveal Lévy flights and superdiffusive long-range transport even though there are no jet regions in the flow (the flow is composed entirely of recirculating zones). Furthermore, we find conditions where the growth of the variance is described by two different values of γ for different time regimes. The shorter time scaling behavior – which is usually not considered theoretically – is likely to be of significant importance for real systems, where issues of practical importance may occur over time scales far short of those needed to achieve the long-time limit common in theories of anomalous diffusion. We propose that this short-time behavior can be explained by considering correlations between flights, which result in clusters that must be considered when relating flight statistics to long-range transport.

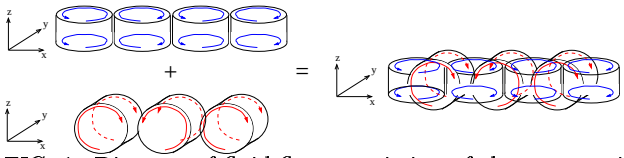

FIG. 1. Diagram of fluid flow, consisting of the superposition of a horizontal chain of alternating vortices with a vertical chain of alternating vortices.

The flow studied is the superposition of two chains of alternating vortices (Fig. 1). The equations describing the velocity field are

$$\dot{x} = -a\frac{\lambda}{2d}cos(\frac{2\pi(x+0.5)}{\lambda})sin(\frac{\pi y}{d}) - a_2\frac{\lambda}{2d_2}cos(\frac{2\pi x}{\lambda})sin(\frac{\pi z}{d_2}) ,$$

$$\dot{y} = asin(\frac{2\pi(x+0.5)}{\lambda})cos(\frac{\pi y}{d}) ,$$

$$\dot{z} = a_2 sin(\frac{2\pi x}{\lambda})cos(\frac{\pi z}{d_2}) .$$

In these equations, a and a_2 are the magnitudes of the two superposed vortex chains, and d and d_2 are the height and width (respectively) of the fluid layer. Throughout the rest of the paper, all lengths are scaled by the vortex width d and times are scaled by a characteristic

turnover time d/a. The relative magnitude of the two vortex chains is denoted by the amplitude ratio a/a_2.

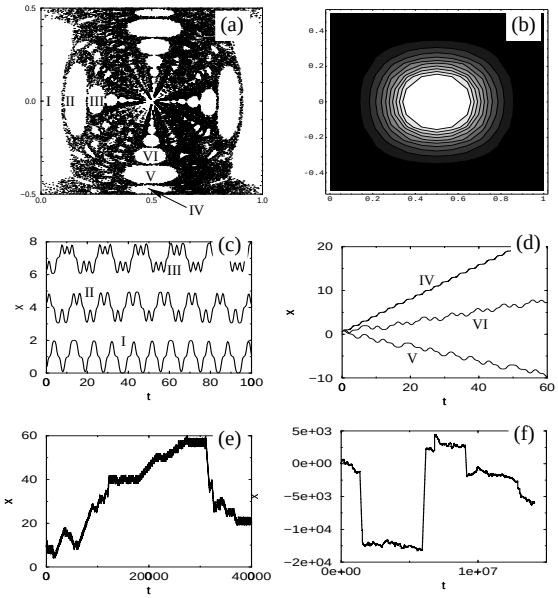

FIG. 2. Results of simulations for $a/a_2 = 5.0$. (a) Poincaré section at $z = 0.0$. (b) Diagnostic $|\vec{\nabla} \times \vec{\omega}|^2$. The white regions correspond to large values of $|\vec{\nabla} \times \vec{\omega}|^2$, where the theory predicts chaotic regions. (c) Sample trapped trajectories from ordered regions. Each curve is labelled with a roman numeral corresponding to an island in Fig. (a). (d) Sample untrapped trajectories from ordered regions. The differing velocities is apparent from the slopes of these curves. (e) and (f) Sample trajectories from chaotic region.

Particle trajectories are determined numerically by integrating these equations using a fourth-order Runge-Kutta technique. The results are shown in Figs. 2 and 3 for $a/a_2 = 5.0$ and 1.0, respectively.

Poincaré sections are plotted in Figs. 2(a) and 3(a). The points in these plots show the x-y coordinates of a single tracer each time it passes through the mid-height ($z = 0$) of the system. Periodic boundary conditions have been used at the left and right. A single tracer in the chaotic region visits the entire region, resulting in an intricate stochastic web for both amplitude ratios with empty "islands" corresponding to regions containing ordered trajectories. Figures 2(b) and 3(b) show the diagnostic proposed by Yannacopoulos et al., as applied to the flow in Eq. (1). It is apparent from the comparison between Figs. (a) and (b) in both cases that the diagnostic works quite well at identifying regions where Lagrangian chaos is most likely to be found.

The x-coordinate of the particle trajectories (plotted in Figs. 2 and 3, (c) - (f)) is the one most relevant to discussions of long-range transport. Figures (c) and (d) in both cases show ordered trajectories for tracers confined to the appropriately-labelled islands in Fig. (a). The oscillatory behavior is due to figure-8 motion between adjacent horizontal vortices, with increasing number of loops for islands near the centers for $a/a_2 = 5.0$.

Of particular importance are the unbounded trajectories, such as those plotted in (d) of Figs. 2 and 3. Tracers undergoing these trajectories travel a very long distance (at least several times longer than a vortex width) in a short period of time, with the average x-velocity determined by the number of loops executed in each vortex before crossing to the next. Tracers in the stochastic region (Figs. (e) and (f)) temporarily stick to the outsides of the islands, [8] mimicking the behavior of the corresponding ordered trajectory while stuck. The sticking process results in flights with a wide range of lengths and durations for all of the chaotic trajectories. It is striking that flights of these lengths are possible in this flow, even though there are no jet regions. Several different flight velocities are possible, depending on which island the tracer is sticking during the flights.

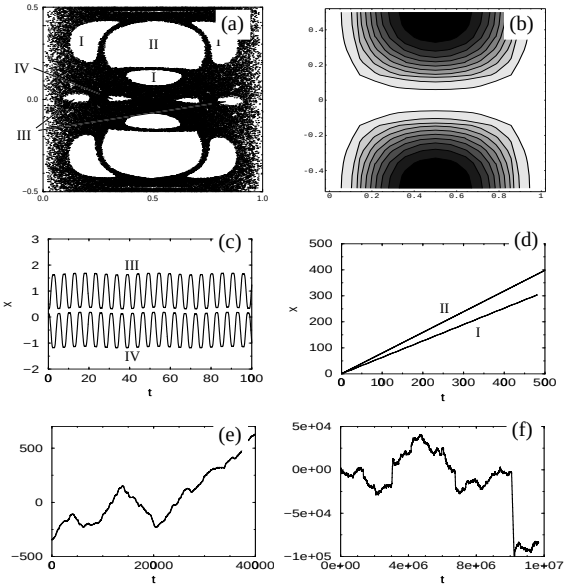

FIG. 3. Results of simulations for $a/a_2 = 1.0$. (a) Poincaré section at $z = 0.0$. (b) Diagnostic $|\vec{\nabla} \times \vec{\omega}|^2$. The white regions correspond to large values of $|\vec{\nabla} \times \vec{\omega}|^2$, where the theory predicts chaotic regions. (c) Sample trapped trajectories from ordered regions. Each curve is labelled with a roman numeral corresponding to an island in Fig. (a). (d) Sample untrapped trajectories from ordered regions. (e) and (f) Sample trajectories from chaotic region.

The variance of a spreading ensemble of tracers is plotted in Figs. 4(a) and (b) for amplitude ratios 5.0 and 1.0, respectively. Superdiffusive transport is evident in both cases. However, whereas the case with $a/a_2 = 5.0$ is characterized by a consistent scaling exponent $\gamma = 1.6 \pm 0.1$ for 2-1/2 orders of magnitude, the case with $a/a_2 = 1.0$ has two well-defined scaling regions: $\gamma = 1.8 \pm 0.1$ for $t < 1600$ (in units of d/a) and $\gamma = 1.5 \pm 0.1$ for $t > 1600$.

Statistics relating to the flights and trapping events are shown in Figs. 5 and 6 for amplitude ratios 5.0 and

1.0, respectively. Flights are identified from the numerical data by analyzing crossings of the separatrices of the horizontal vortices. Each flight has a velocity defined as distance travelled per unit time. When considering separatrix crossings, a particular velocity can easily be characterized by the number of repeated crossings of a particular separatrix before the tracer continues on to the next one. A flight is considered to end if the magnitude of the velocity changes or if the tracer reverses direction.

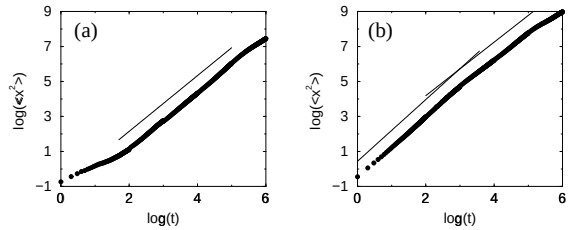

FIG. 4. Growth of the variance of a distribution. Fits (thin solid lines) show the scaling regions; all fits are raised by 1 unit to distinguish from the data. (a) Amplitude ratio $a/a_2 = 5.0$; slope is 1.6 ± 0.1 from log(t) = 2.0 to 4.6. (b) $a/a_2 = 1.0$; slope is 1.8 ± 0.1 from log(t) = 1.0 to 3.2 and 1.5 ± 0.1 from log(t) = 3.2 to 5.2.

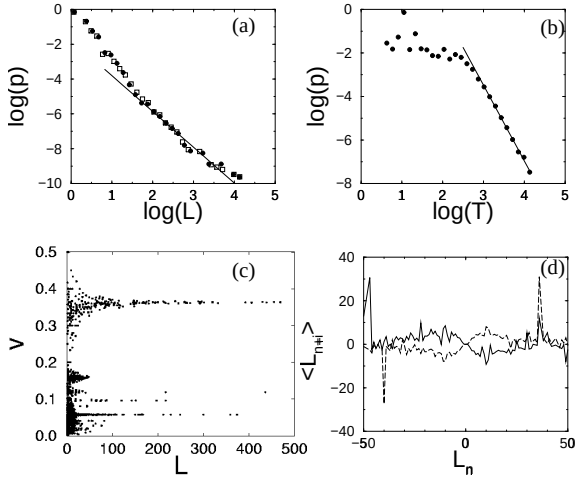

FIG. 5. Statistics for flights and trapping events for amplitude ratio $a/a_2 = 5.0$. (a) Probability distribution function (PDF) for flight length (filled circles), along with best fit; slope $= -2.2 \pm 0.3$. The open squares correspond to the PDF of lengths of flight clusters. (b) PDF for trapping durations, along with best fit; slope $= -3.5 \pm 0.2$; (c) Scatter plot of flight length L and speed v. (d) Correlations between flights; average length for next flight (n+1 – solid line) and for following flight (n+2 – dashed line).

Plots of the probability distribution functions (PDFs) for flight length are shown in part (a) of Figs. 5 and 6 (filled circles). The PDFs have algebraic tails, indicating divergence of the second moment of the distribution: $< L^2 > \to \infty$ and $< T^2 > \to \infty$, consistent with the definition of a Lévy flight. Specifically, the flight lengths scale as $p(L) \sim L^{-\mu_L}$ with $\mu_L = 2.2 \pm 0.3$ and 2.6 ± 0.3 for amplitude ratios 5.0 and 1.0, respectively. (The flight durations – not shown – scale as $p(T) \sim T^{-\mu_T}$ with $\mu_T = 2.8 \pm 0.2$ and 3.0 ± 0.2 for ratios 5.0 and 1.0, respectively.)

Trapping duration PDFs (Figs. 5b and 6b) also have algebraic tails, but with exponents $\nu = 3.5$ and 4.2 (± 0.2) for amplitude ratios of 5.0 and 1.0, respectively. These exponents are both greater than 3; consequently, the trapping durations both have finite second moment and are therefore not described as Lévy distributions.

Theories have been developed that relate the growth of the variance to flight and trap statistics. In particular, detailed predictions have been made [9] for the case where flights all have the same constant velocity. In the regime where the trapping exponent $\nu > 3$ (as is the case here), the variance is predicted to grow as $< x^2 > \sim t^\gamma$ with $\gamma = 2$ for $\mu < 2$, $\gamma = 4 - \mu$ for $2 < \mu < 3$ and $\gamma = 1$ for $\mu > 3$. In the data presented here, for both amplitude ratios the long time behavior of the growth exponent γ is consistent with these predictions.

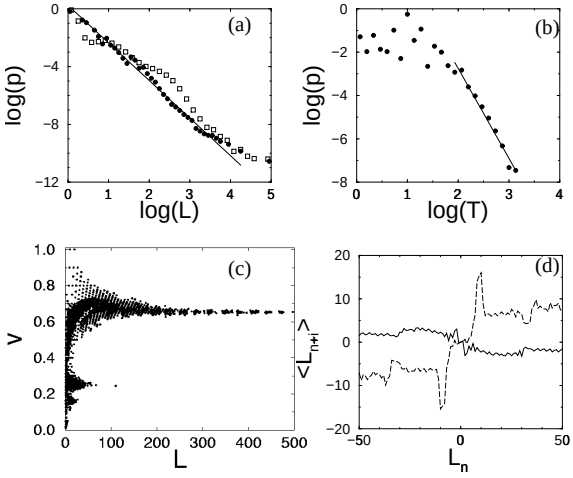

FIG. 6. Statistics for flights and trapping events for amplitude ratio $a/a_2 = 1.0$. (a) Probability distribution function (PDF) for flight length (filled circles), along with best fit; slope $= -2.6 \pm 0.3$. The open squares correspond to the PDF of lengths of flight clusters. (b) PDF for trapping durations, along with best fit; slope $= -4.2 \pm 0.2$; (c) Scatter plot of flight length L and speed v. (d) Correlations between flights; average length for next flight (n+1 – solid line) and for following flight (n+2 – dashed line).

Despite the success of the theory in relating the long-time scaling of the variance with the flight statistics, there are some important deviations between the models used in those theories and the current system. First, whereas the theories [9] assume constant velocity flights, in this system different flights have different velocities. This fact is revealed in scatter plots of flight length versus

speed, as is shown in Figs. 5c and 6c. A few dominant speeds are apparent for the shorter length flights, each speed corresponding to sticking of trajectories to a different island in the Poincaré sections of Figs. 2 and 3. Fewer of the islands are able to maintain the longer flights, however, evidenced by the dropping out of some of the velocities as the flight length increases. For the $a/a_2 = 1.0$ case in particular (Fig. 6c), flights with lengths greater than 50 vortex widths are dominated by a single flight velocity. The implication of these results is that each island may be associated with its own PDF for sticking and that, in general, characterization of the flights with a single flight length PDF may result in an incomplete description of the phenomena. The success of the theories [9] in predicting the long-time behavior for this system stems from the fact that the long flights are dominated by a single velocity.

Another deviation from the standard theoretical models stems from the fact that the flights observed in these simulations are not independent. In fact, there are significant correlations between a flight and the subsequent two flights, as shown in Figs. 5d and 6d. For an amplitude ratio of 5.0 (Fig. 5d), there is an increased probability that a flight will be followed by another flight in the opposite direction, as shown by the dashed line. The following flight, however, has an equivalent average magnitude in the direction of the original (L_n) flight. For an amplitude ratio of 1.0 (Fig. 6d), however, there is a stronger correlation with flights in the same direction for the second flight than for flights in the opposite direction for the next flight. The result is that flights tend to cluster for an amplitude ratio of 1.0, with the clusters having a larger overall length than the individual flights.

The PDFs of the lengths of flight clusters are denoted by open squares in the plots of the flight length PDFs (Figs. 5a and 6a). Whereas the statistics for the clusters are the same as for the individual flights for $a/a_2 = 5.0$ (Fig. 5a), there is a significant difference between the flight and cluster length PDFs for $a/a_2 = 1.0$ (Fig. 6a). For $t < 1000$ ($log(t) < 3$), the cluster PDF decays with a significantly smaller exponent (1.6 ± 0.3), then drops down for larger t, following the same scaling for the larger lengths. The slow drop-off for $t < 10^3$ explains the almost ballistic (γ near 2) growth of the variance for $t < 10^3$ in Fig. 4b.

The implication here is that the statistics of the flights alone are not sufficient to determine the long-range transport behavior if the flights have significant correlations. An analysis based on flight clusters gives a better prediction of the scaling behavior of the variance of a distribution.

Experiments are currently in progress to test these results. In the experiments, the horizontal chain of vortices is producd by a magnetohydrodynamic technique, [10] while the vertical vortices are generated by thermal convection from heating and cooling strips. Preliminary results show trajectories that are qualitatively similar to those from the simulations. More data is needed to make quantitative comparisons, though. This will be the subject of a future article.

We are pleased to acknowledge discussions with Igor Mezic. These studies are supported by NSF grants PHY-9732158 and DMR-0071771. Equipment used in these studies was funded by a Cottrell College Science Award of Research Corporation.

---

* Electronic mail: tsolomon@bucknell.edu

† Current address: Department of Mechanical and Aerospace Engineering, Cornell University. Electronic mail: fogleman@mae.cornell.edu

[1] H. Aref, J. Fluid Mech. **143**, 1 (1984); J.M. Ottino, *The Kinematics of Mixing: Stretching, Chaos, and Transport* (Cambridge University Press, Cambridge, 1989).

[2] For a review, see H. Aref, Phil. Trans. Roy. Soc., **A333**, 273 (1990).

[3] T.H. Solomon, S. Tomas, and J.L. Warner, Phys. Rev. Lett. **77**, 2682 (1996).

[4] V.I. Arnold, C. R. Acad. Sci. Paris **261**, 17 (1965).

[5] A. N. Yannacopoulos, I. Mezic, G. Rowlands, and G. P. King, Phys. Rev. E **57**, 482 (1998).

[6] E.W. Montroll and M.F. Shlesinger, in *Nonequilibrium Phenomena II: From Stochastics to Hydrodynamics*, Studies in Statistical Mechanics Vol. II, edited by J. L. Lebowitz and E.W. Montroll (North-Holland, Amsterdam, 1984), p. 1; M.F. Shlesinger, G.M. Zaslavsky, and J. Klafter, Nature **363**, 31 (1993).

[7] T.H. Solomon, E.R. Weeks, and H.L. Swinney, Phys. Rev. Lett. **71**, 3975 (1993); T.H. Solomon, E.R. Weeks, and H.L. Swinney, Physica D **76**, 70 (1994).

[8] M. Ding, T. Bountis, and E. Ott, Phys. Lett. A **151**, 395 (1990); Y.-C. Lai, M. Ding, C. Grebogi, and R. Blümel, Phys. Rev. A **46**, 4661 (1992); G.M. Zaslavsky, D. Stevens, and H. Weitzner, Phys. Rev. E **48**, 1683 (1993).

[9] J. Klafter, A. Blumen, and M.F. Shlesinger, Phys. Rev. A **35**, 3081 (1987); X.-J. Wang, Phys. Rev. A **45**, 8407 (1992); M.F. Shlesinger, J. Stat. Phys. **10**, 421 (1974); J. Klafter and G. Zumofen, Phys. Rev. E **49**, 4873 (1994); E.R. Weeks and H.L. Swinney, Phys. Rev. E **57**, 4915 (1998).

[10] H. Willaime, O. Cardoso, and P. Tabeling, Phys. Rev. E **48**, 288 (1993); T.H. Solomon, S. Tomas, and J.L. Warner, Phys. Fluids **10**, 342 (1998).